Journal of Pathology
J Pathol April 2021; **253:** 404–414
Published online 31 January 2021 in Wiley Online Library (wileyonlinelibrary.com) DOI: 10.1002/path.5605

ORIGINAL PAPER

The dysregulation of metabolic pathways and induction of the pentose phosphate pathway in renal ischaemia–reperfusion injury

Angelique ML Scantlebery[1]*, Alessandra Tammaro[1], James D Mills[1], Elena Rampanelli[2], Lotte Kors[1], Gwendoline J Teske[1], Loes M Butter[1], Gerhard Liebisch[3], Gerd Schmitz[3], Sandrine Florquin[1], Jaklien C Leemans[1] and Joris JTH Roelofs[1,4]

[1] *Department of Pathology, Amsterdam Infection and Immunity Institute, Amsterdam University Medical Center (Location AMC), Amsterdam, The Netherlands*
[2] *Department of Experimental Vascular Medicine, Amsterdam University Medical Center (Location AMC), Amsterdam, The Netherlands*
[3] *Institute of Clinical Chemistry and Laboratory Medicine, University Hospital of Regensburg, Regensburg, Germany*
[4] *Amsterdam Cardiovascular Sciences, Amsterdam University Medical Center (Location AMC), Amsterdam, The Netherlands*

**Correspondence to: AML Scantlebery, Department of Pathology – Renal Injury and Repair, Amsterdam UMC – University of Amsterdam, Meibergdreef 9, 1105 AZ Amsterdam, The Netherlands. E-mail: a.m.scantlebery@amsterdamumc.nl*

Abstract

Lipid accumulation is associated with various forms of acute renal injury; however, the causative factors and pathways underpinning this lipid accumulation have not been thoroughly investigated. In this study, we performed lipidomic profiling of renal tissue following ischaemia–reperfusion injury (IRI). We identified a significant accumulation of cholesterol and specific phospholipids and sphingolipids in kidneys 24 h after IRI. In light of these findings, we hypothesised that pathways involved in lipid metabolism may also be altered. Through the analysis of published microarray data, generated from sham and ischaemic kidneys, we identified nephron-specific metabolic pathways affected by IRI and validated these findings in ischaemic renal tissue. *In silico* analysis revealed the downregulation of several energy and lipid metabolism pathways, including mitochondrial fatty acid beta-oxidation (FAO), peroxisomal lipid metabolism, fatty acid (FA) metabolism, and glycolysis. The pentose phosphate pathway (PPP), which is fuelled by glycolysis, was the only metabolic pathway that was upregulated 24 h following IRI. In this study, we describe the effect of renal IRI on metabolic pathways and how this contributes to lipid accumulation.

Keywords: ischaemia–reperfusion injury; kidney; lipid accumulation; lipid metabolism; energy metabolism; fatty acid beta-oxidation; pentose phosphate pathway

Received 16 June 2020; Revised 1 December 2020; Accepted 14 December 2020

No conflicts of interest were declared.

Introduction

Renal ischaemia–reperfusion injury (IRI) is a pertinent issue in sepsis [1], major surgery [2], and shock [3], but also renal transplantation, as it has been established as a risk factor for acute kidney injury (AKI), delayed graft function (DGF), and both acute and chronic rejection [4]. IRI is defined as a temporary, concomitant deprivation of oxygen and nutrients, resulting in reduced oxidative phosphorylation (OXPHOS), ATP depletion, and metabolic waste accumulation [5].

Neutral lipid accumulation, a well-established feature of many forms of renal injury, is observed after IRI. Zager *et al* observed cortical cholesterol and triacylglycerol (TAG) accumulation following several forms of AKI. Even physiological stress, which does not result in renal tubular damage, was also found to cause lipid deposition [6–8]. This suggests that lipid accumulation is not simply an effect of tubular damage, but a component of the cellular stress response. Our group has shown that renal lipid accumulation is not restricted to neutral lipids. Metabolic overload in mice leads to an increase in cholesterol and phospholipids in the proximal tubules, illustrating the kidney's susceptibility to both polar and nonpolar lipid accumulation [9]. We found diet-induced renal lipid accumulation to be associated with renal damage, inflammation, and fibrosis in mice [9]; however, the effect of lipid accumulation on renal tissue remains a topic of debate. Zager's group coined the term 'acquired renal cytoresistance' (ACR) after demonstrating that various forms of renal injury conferred resistance to a secondary insult of the same nature [10,11]. They later reported that all cytoresistant responses were associated with increased renal cortical cholesterol, and inhibition of cholesterol synthesis *in vitro* prevented the development of ACR in proximal tubules [12].

Lipid accumulation is clearly a common phenotype following renal injury; however, similar to the uncertainties regarding its damaging or beneficial effect, the underlying cause of this phenomenon also requires further study. As ischaemia is known to suppress OXPHOS [13], a major energy-producing metabolic pathway in the kidney, it is plausible that pathways associated with lipid metabolism could also be affected by an ischaemic event. Our aim was to investigate the alterations in lipid profile and the underlying metabolic pathway rewiring that occurs during IRI. In order to further characterise the renal lipid profile following IRI, we performed mass spectrometry (MS) lipidomic analysis of kidney tissues and found an accumulation of cholesterol and specific phospholipids and sphingolipids in the early stages of IRI-induced AKI. Additionally, through an *in silico* analysis of published datasets, we analysed changes in metabolic pathways in response to IRI and validated these findings in our own IRI model. We found that major energy and lipid metabolism pathways were downregulated following IRI. The pentose phosphate pathway (PPP) was the only metabolic pathway that was upregulated 24 h following IRI, suggesting that this pathway may be beneficial for adaptive repair.

Materials and methods

Mice

Pathogen-free, wild-type (WT), male C57BL/6J mice, 8–12 weeks of age, were purchased from Charles River Laboratories (Cologne, Germany) for the purpose of ischaemia–reperfusion experiments. Animals were housed in the animal care facility of the Academic Medical Center (University of Amsterdam) in accordance with national guidelines and given *ad libitum* access to both food and water. Environmental conditions were monitored daily. These were in compliance with the criteria set by the American Association for Laboratory Animal Science (AALAS). All experiments were approved by the Animal Care and Use Committee of the University of Amsterdam.

Ischaemia–reperfusion injury

Renal ischaemic insult was induced by unilateral clamping of the renal pedicle ($n = 5$) or bilateral clamping of both pedicles ($n = 7$). In brief, either the left or both renal arteries were clamped for 20 min through an incision in the flank under general anaesthesia (2.25% isoflurane–100% oxygen). Upon removal of the clamp, the incision was closed in two layers, and mice received Temgesic (0.1 mg/kg buprenorphine; Schering-Plough BV, Amstelveen, The Netherlands), administered by subcutaneous injection. A sham group ($n = 4$) received a similar incision in the flank without renal clamping. All mice were sacrificed 24 h after surgery by means of exsanguination and cervical dislocation, all performed under general anaesthesia (isoflurane). Kidneys were snap-frozen in liquid nitrogen and/or fixed in neutral-buffered formalin in preparation for further analyses.

Kidney histology

Formalin-fixed, paraffin-embedded renal sections (4 μm thick) were stained using periodic acid–Schiff–diastase (PAS-D), as described previously [14], for the general visualisation of renal histology.

For the visualisation of lipid droplets (LDs), renal sections were pretreated for optimal epitope-retrieval, as described previously [14]. Tissue was stained with guinea pig anti-perilipin-2 primary antibody (Progen Biotechnik, Heidelberg, Germany; Cat # GP40, 1:10 000), followed by incubation with a secondary rabbit anti-guinea pig (Thermo Scientific, Waltham, MA, USA) antibody and a final incubation with a tertiary layer, peroxidase-labelled antibody (Powervision poly HRP-anti rabbit; Immunologic, Duiven, The Netherlands), prior to visualisation with the DAB Plus system (Dako, Glostrup, Denmark).

Mass spectrometry

Lipids were extracted from homogenised tissues by Bligh and Dyer's chloroform/methanol extraction method [15]. Analysis was performed by direct flow injection electrospray ionisation tandem mass spectrometry (ESI–MS/MS) in positive ion mode, using the analytical setup and strategy described previously [16]. Sphingolipids and minor glycerophospholipids were extracted by the butanolic extraction procedure as described by Baker *et al* [17] and Scherer *et al* [18] and analysed by liquid chromatography–tandem mass spectrometry (LC–MS/MS), as described previously [19]. Quantification was attained utilising non-naturally occurring internal standards and calibration lines generated by standard addition of a number of naturally occurring species to samples. Excel Macros made in-house were employed for deisotoping and data analysis of all lipid classes [17–21]. Annotation of glycerophospholipid species was based on the presupposition that the fatty acyls contain an even number of carbon atoms. Sphingomyelin species were assigned based on the assumption of a sphingoid base with two hydroxyl groups.

Microarray data

In 2014, Liu *et al* published an article in which they described how they were able to measure gene expression in specific cell populations within the kidney following bilateral IRI [22]. This microarray dataset was retrieved from NCBI Geo Datasets under the accession number GSE52004. The retrieved microarray dataset had already been normalised using the robust multi-array average (RMA) approach. From this database, we used gene expression data measured in cells from the nephron both 4 h and 24 h following reperfusion. Data from sham mice were used as a control. Each group contained expression data from three mice.

Microarray data analysis

Analysis of the microarray data was carried out using Bioconductor packages in the R statistical programming language. The normalised microarray dataset was $\log_2$ transformed and passed to the R package 'limma' for differential expression analysis [23]. First, the fold-changes and standard errors were estimated by fitting a linear model for each gene. Next, an empirical Bayes method was used to moderate the standard errors towards a common value and a moderated *t*-statistic was calculated. Genes with a Benjamini–Hochberg adjusted *P* value less than 0.05 were considered statistically significant.

The genes that were considered differentially expressed were passed to the R package ReactomePA for pathway enrichment analysis [24]. The ReactomePA package allows for enrichment analysis using the reactome pathway database [25]. Those pathways with a Benjamini–Hochberg adjusted *P* value less than 0.05 were considered significant. The top 30 enriched reactome pathways were visualised as an enrichment map using an inbuilt function in the ReactomePA package.

Heatmaps

Pathway analysis identified differential expression of functionally related genes. To determine whether these pathways were up- or downregulated, custom heatmaps were generated using the NetworkAnalyst 3.0 analytics platform [26]. Gene expression was shown for sham mice and mice sacrificed 4 and 24 h following reperfusion.

Reverse transcription-quantitative PCR (RT-qPCR)

Total RNA was isolated from 300-µm-thick frozen renal sections using TRIzol reagents (Invitrogen, Breda, The Netherlands). RNA isolation was performed according to the manufacturer's instructions. Complementary DNA was generated following a standard protocol. In brief, oligo-dT primers were annealed to the RNA for 10 min at 72 °C, followed by reverse transcription for 60 min at 37 °C using M-MLV reverse transcriptase (Promega, Leiden, The Netherlands). Real-time cDNA quantification was performed on the Roche LightCycler 480 (Roche Diagnostics, Almere, The Netherlands) using a SensiFAST SYBR No-ROX kit (Bioline, Waddinxveen, The Netherlands). Gene expression was normalised against TATA-box binding protein (*Tbp*) transcripts. Analysis was performed using the LinRegPCR 12.4 software. The following genes were analysed: *Havcr1* (kidney injury marker-1; *Kim-1*), *Lcn2* (neutrophil gelatinase-associated lipocalin; *Ngal*), *Ppara* (peroxisome proliferator-activated receptor-alpha), *Ppargc1a* (peroxisome proliferator-activated receptor gamma coactivator 1-alpha; *Pcg1-alpha*), *G6pdx* (glucose-6-phosphate dehydrogenase X), *Taldo1* (transaldolase 1), *Tkt* (transketolase), *Prps1* (phosphoribosyl pyrophosphate synthetase 1), *Fasn* (fatty acid synthase), and *Cd36* (cluster of differentiation 36). Primer sequences are listed in supplementary material, Table S1.

Statistical analyses

Statistical analysis was performed using Graphpad Prism 8.3 software (Graphpad Software, San Diego, CA, USA) and data are presented as mean ± SEM. Datasets were tested for normality using the Shapiro–Wilk normality test. Based on data distribution, statistical analysis was then performed using an unpaired *t*-test or a Mann–Whitney test. Outliers were determined using Grubbs' test and subsequently excluded.

Results

Lipidomic profiling in ischaemic kidneys

In order to understand the diversity in lipid accumulation following renal IRI, we performed MS-based lipidomics on renal tissue from our unilateral IRI model. Tissue was harvested 24 h post-ischaemia, the time point at which tubular necrosis and intratubular cast formation occur (supplementary material, Figure S1A). An extensive panel of major sterols [cholesteryl esters (CE) and free cholesterol (FC); Figure 1A,B], phospholipids [phosphatidylcholine (PC), phosphatidylglycerol (PG), phosphatidylinositol (PI), and bis(monoacylglycero) phosphate (BMP); Figure 1C–F], and sphingolipids [sphingomyelin (SM), dihydrosphingomyelin (DSM), ceramide (Cer), hexosylceramide (HexCer), sphinganine (SPA), and sphingosine (SPH); Figure 2] was measured.

Cholesteryl esters, together with TAG and diacylglycerol (DAG), are stored intracellularly in lipid droplets (LDs) [27]. Therefore, we assessed the abundance of LDs. Staining for perilipin-2, a structural component of the LD outer layer, showed the presence of LDs within ischaemic tubules. Perilipin-2 positivity was negligible in sham kidneys (supplementary material, Figure S1B). As excess fatty acids (FAs) are stored as TAGs, renal expression of genes encoding for CD36, the tubular FA uptake molecule, and FASN, the enzyme that catalyses FA synthesis, was measured. The expression of both genes was significantly decreased upon IRI (supplementary material, Figure S1C,D).

Ischaemic kidneys displayed a significant increase in both CE and FC (Figure 1A,B), as well as a trend towards increased phospholipid levels (Figure 1C–F), with a statistically significant increase being observed for PG (Figure 1D). Measurements were also performed for phosphatidylethanolamine (PE) and phosphatidylserine (PS), which were found to be unaffected by IRI (data not shown). Among the sphingolipids analysed, DSM, Cer, HexCer, and SPH levels were significantly increased in ischaemic kidneys (Figure 2). In addition, SPA and SM levels were increased in ischaemic kidneys, but did not reach statistical significance (Figure 2).

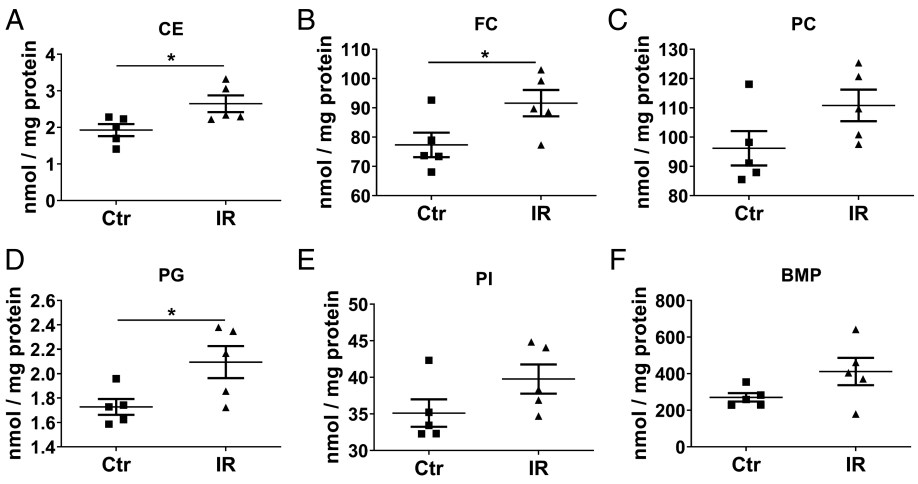

Figure 1. Effect of IRI on renal cholesterol and phospholipid content. Mass spectrometry analysis of renal homogenates from contralateral kidneys and ischaemic kidneys 24 h following IRI (unilateral IRI model). Lipid quantifications were performed for (A, B) cholesterols: CE and FC, and (C–F) phospholipids: PC, PG, PI, and BMP. Data shown as mean ± SEM. CE, cholesteryl esters; FC, free cholesterol; PC, phosphatidylcholine; PG, phosphatidylglycerol; PI, phosphatidylinositol; BMP, bis(monoacylglycerol)phosphate; Ctr, contralateral kidney; IR, ischaemia–reperfusion. Statistical analysis for PI was performed using a Mann–Whitney test. Unpaired *t*-tests were used for all other lipids. $^{*}p \leq 0.05$.

Network map of pathways in the nephron affected by IRI

As IRI is known to affect renal energy metabolism, we performed a broad investigation to identify pathways affected by IRI, hypothesising that we would encounter pathways that could be associated with lipid accumulation. We performed *in silico* analysis of published microarray data (GSE52004) generated from analysis of

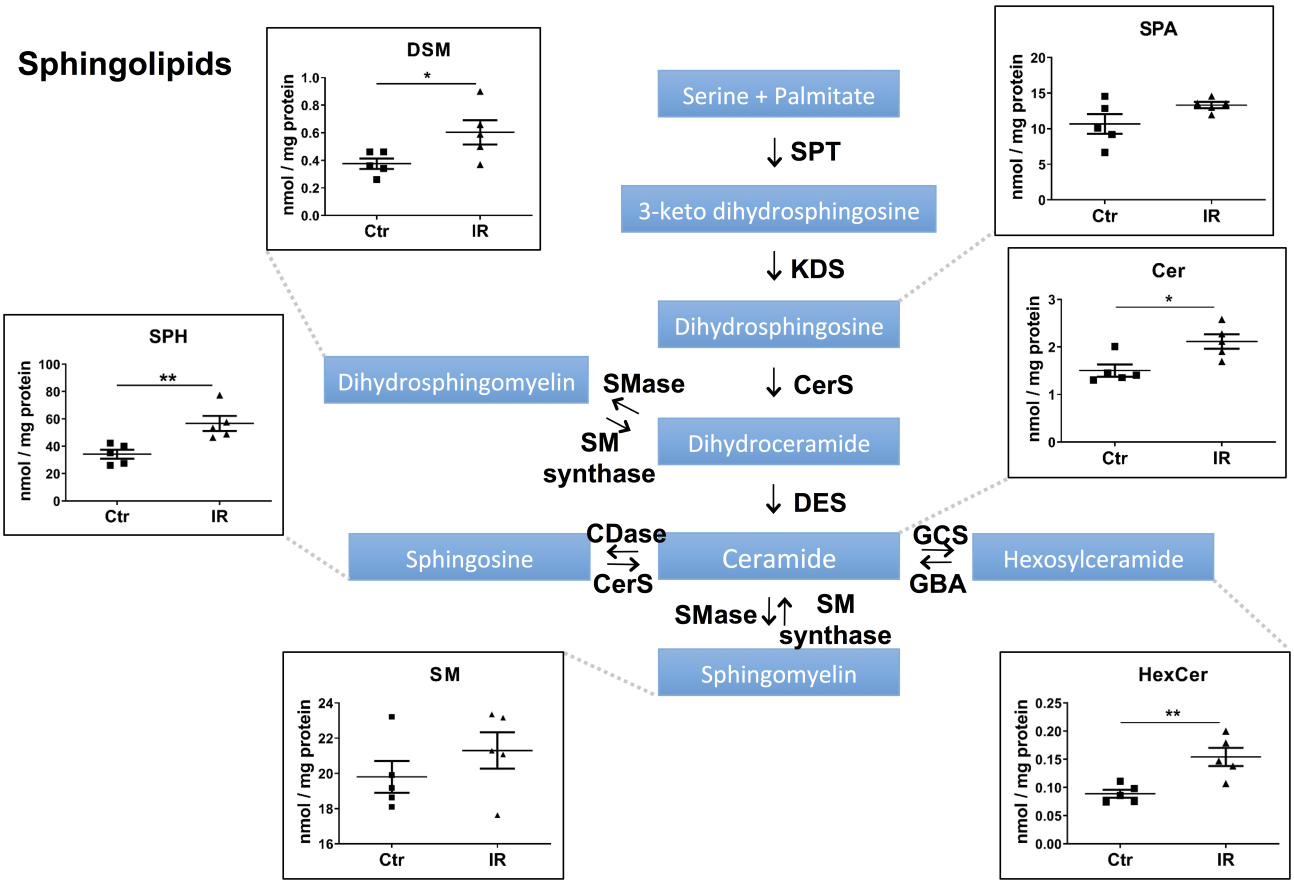

Figure 2. Effect of IRI on renal sphingolipid content. Mass spectrometry analysis of renal homogenates from contralateral kidneys and ischaemic kidneys 24 h following IRI (unilateral IRI model). Lipid quantifications were performed for several sphingolipid intermediates. Data shown as mean ± SEM. SPA, sphinganine; DSM, dihydrosphingomyelin; Cer, ceramide; HexCer, hexosylceramide; SM, sphingomyelin; SPH, sphingosine; Ctr, contralateral kidney; IR, ischaemia–reperfusion. Statistical analysis for Cer was performed using a Mann–Whitney test. Unpaired *t*-tests were used for the statistical analysis of all other lipids. $^{*}p \leq 0.05$, $^{**}p \leq 0.01$.

murine kidneys harvested 24 h after bilateral IRI or sham surgery. This dataset was chosen as it contains cell type-specific data, allowing the identification of pathways affected in the nephron following IRI, while excluding the interference of vascular and inflammatory cells. The extent of the renal injury can be assessed in the supplemental data shown in the original article [22]. Gene pathway enrichment analysis and network mapping were used to visualise pathways in which a significant change in gene expression was measured. Major differences in the expression of genes involved in pathways related to transcription, cell cycle, lipid metabolism, and energy metabolism were observed in ischaemic kidneys when compared with sham controls (supplementary material, Figure S2). Therefore, we studied next the expression of genes crucial for energy and lipid metabolism pathways.

Effect of IRI on the expression of genes involved in metabolic pathways in the nephron

The NetworkAnalyst platform was used to generate heatmaps to visualise the expression of the genes involved in the IRI-affected pathways, both 4 h and 24 h post-IRI (Figures 3–5). For the purpose of this article, we focused on pathways involved in energy and lipid metabolism. IRI was found to lower the expression of genes involved in the tricarboxylic acid (TCA) cycle, respiratory electron transport (supplementary material, Figures S3 and S4), mitochondrial fatty acid beta-oxidation (FAO) (Figure 3A), and peroxisomal lipid metabolism (Figure 3B). We also analysed data available from mice sacrificed 4 h post-ischaemia to determine if this metabolic change was an early event. Interestingly, gene expression in metabolic pathways appeared to increase (slightly) 4 h after IRI, before decreasing at the 24 h time point. This pattern was observed for all pathways, suggesting that ischaemia does not lead to an immediate metabolic shutdown and that metabolic disruption occurs later in the reperfusion phase along with extensive tubular injury [28].

Due to the sheer number of IRI-affected pathways, it was not feasible for all of them to be displayed in the network map. Therefore, we manually analysed the raw microarray data to find other relevant pathways that were significantly affected by IRI. As mitochondrial FAO was repressed in ischaemic kidneys, we were curious as to whether this would affect general FA metabolism. Indeed, expression of FA metabolism-related genes was downregulated 24 h, but not 4 h, following IRI (Figure 4 and supplementary material, Figure S5). Furthermore, we questioned whether the glycolytic pathway would compensate for the repression of FAO, in order to meet energy requirements. Although the glycolytic

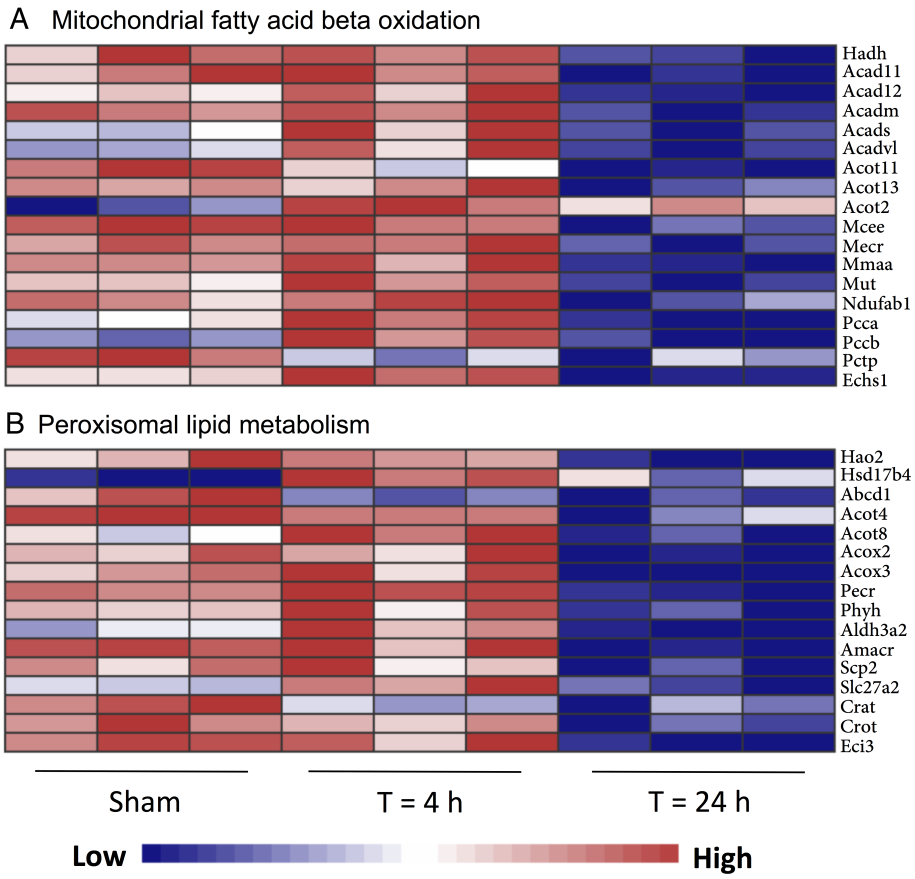

Figure 3. Effect of IRI on the expression of genes involved in metabolic pathways in the nephron (1). Gene expression data, derived from the GSE52004 database, were analysed in renal IRI samples (bilateral IRI model). The NetworkAnalyst platform was used to generate heatmaps to visualise the expression of genes involved in (A) mitochondrial fatty acid beta-oxidation and (B) peroxisomal lipid metabolism pathways.

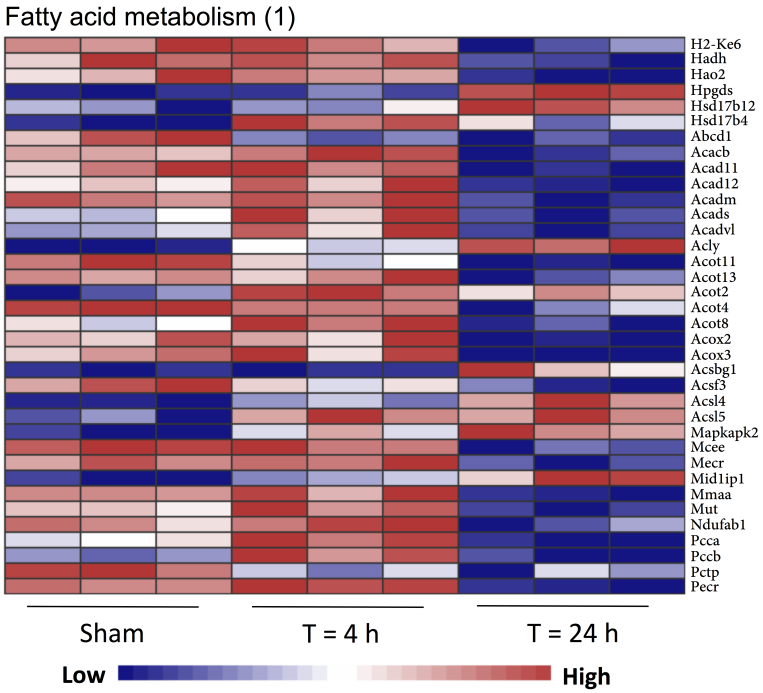

Figure 4. Effect of IRI on the expression of genes involved in metabolic pathways in the nephron (2). Gene expression data, derived from the GSE52004 database, were analysed in renal IRI samples (bilateral IRI model). The NetworkAnalyst platform was used to generate heatmaps to visualise the expression of genes involved in fatty acid metabolism. The remainder of the genes that were differentially expressed in this pathway are shown in supplementary material, Figure S5.

pathway was not listed as a pathway significantly affected by IRI, we compiled a list of glycolytic genes and checked for their expression levels within the microarray data. Interestingly, genes involved in the glycolytic pathway were also found to be downregulated 24 h following IRI (Figure 5A). Similar to the other metabolic pathways, genes relevant for FA metabolism and glycolysis were (slightly) increased at the 4 h time point, before decreasing at the 24 h time point. Upon further analysis of the data, we found the expression of genes involved

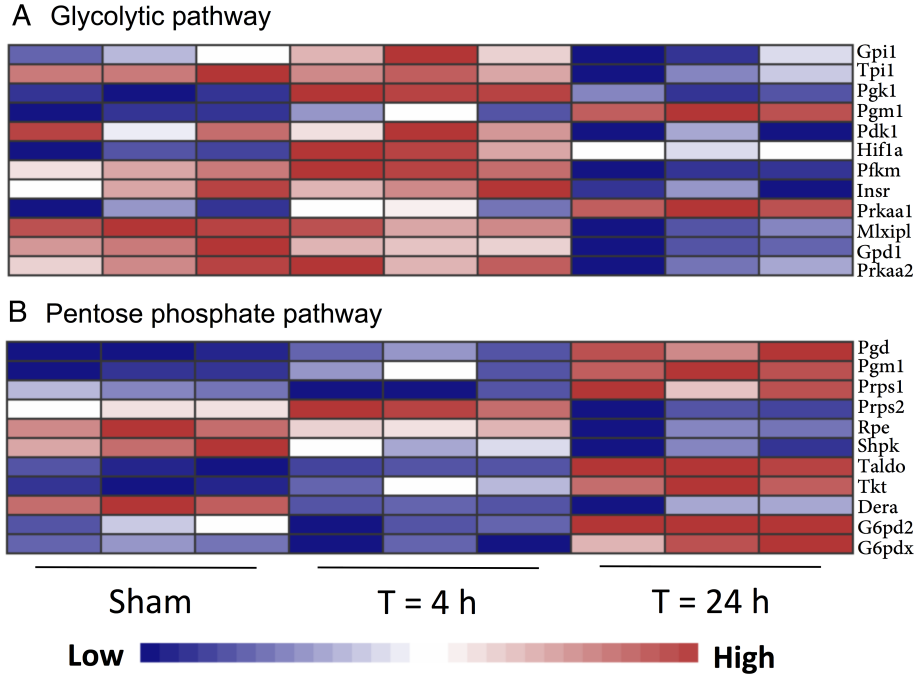

Figure 5. Effect of IRI on the expression of genes involved in metabolic pathways in the nephron (3). Gene expression data, derived from the GSE52004 database, were analysed in renal IRI samples (bilateral IRI model). The NetworkAnalyst platform was used to generate heatmaps to visualise the expression of genes involved in (A) the glycolytic pathway and (B) the pentose phosphate pathway.

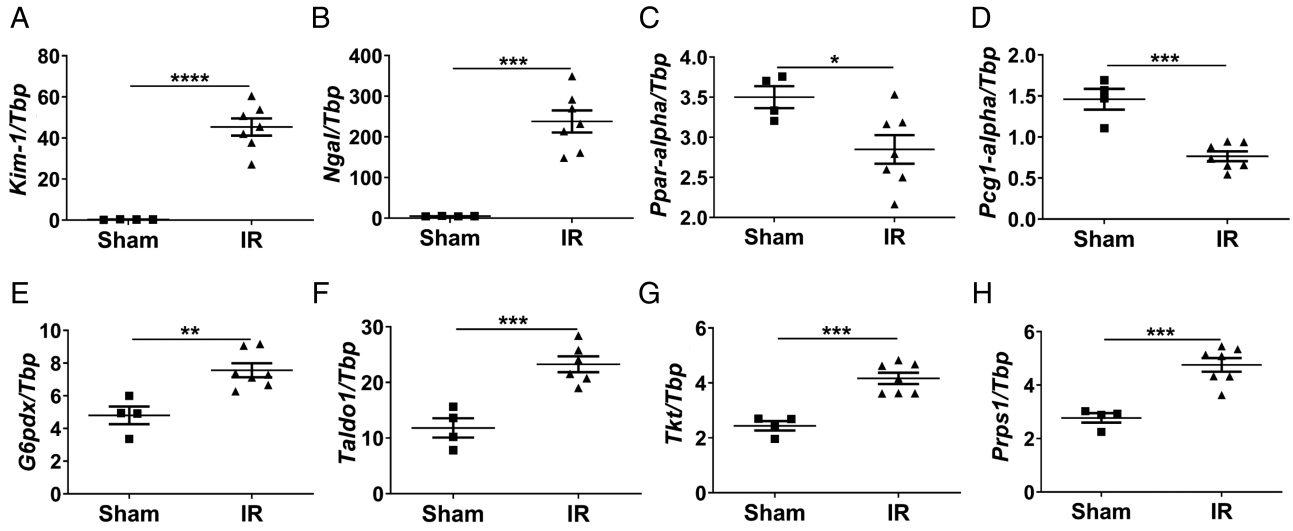

Figure 6. RT-qPCR analysis used to validate the effect of IRI on damage, FAO, and the PPP in the kidney. Gene expression was measured in sham mice and mice sacrificed 24 h following IRI (bilateral IRI model). RT-qPCR analysis was used to measure the expression of genes involved in (A, B) renal damage: *Kim-1* and *Ngal*; (C, D) FAO: *Ppar-alpha* and *Pcg1-alpha*; and (E–H) the PPP: *G6pdx*, *Taldo1*, *Tkt*, and *Prps1*. Data shown as mean ± SEM. *Kim-1*, kidney injury marker-1; *Ngal*, neutrophil gelatinase-associated lipocalin; *Ppar-alpha*, peroxisome proliferator-activated receptor-alpha; *Pcg1-alpha*, peroxisome proliferator-activated receptor gamma coactivator 1-alpha; *G6pdx*, glucose-6-phosphate 1-dehydrogenase; *Taldo1*, transaldolase 1; *Tkt*, transketolase; *Prps1*, ribose-phosphate diphosphokinase 1. Statistical analysis was performed using unpaired *t*-tests for all measurements. $^{*}p \le 0.05$, $^{**}p \le 0.01$, $^{***}p \le 0.001$, $^{****}p \le 0.0001$.

in the pentose phosphate pathway (PPP) to be unaltered at the 4 h time point, but increased at the 24 h time point, when compared with sham controls. In our analysis, the PPP was the only metabolic pathway found to be upregulated in ischaemic kidneys 24 h following injury (Figure 5B). The PPP has been depicted schematically in supplementary material, Figure S6.

RT-qPCR validation of the effect of IRI on damage, FAO, and the PPP in the kidney

We validated the microarray data in kidney samples from our bilateral IRI model that were harvested 24 h following injury. We focused on this time point as both damage and lipid accumulation were observed 24 h following IRI (supplementary material, Figure S1). We evaluated the expression of genes involved in renal damage, FAO, and the PPP. The expression levels of tubular damage markers, *Kim-1* and *Ngal*, were significantly increased in ischaemic mice compared with sham mice (Figure 6A,B). PPAR-alpha and PCG1-alpha are transcription factors whose target genes are involved in FAO. The expression of these FAO-regulating genes, *Ppar-alpha* and *Pcg1-alpha*, was significantly decreased in ischaemic kidneys, indicating suppression of the FAO pathway (Figure 6C,D). Consistent with the results obtained in the *in silico* analysis, the expression of PPP-related genes – *G6pdx*, *Taldo1*, *Tkt*, and *Prps1* – was significantly increased in ischaemic mice, compared with sham mice (Figure 6E–H). It is important to note that elevated expression of PPP-related genes was also observed during the repair phase in a publicly available single cell RNA dataset [29] (supplementary material, Figure S7E–H).

Discussion

Acute renal injury is known to be associated with an increase in renal lipid content. Specifically, cholesterol and TAG levels are increased following AKI [7]. Reports investigating the underlying cause of renal lipid accumulation in AKI are scarce. In this study, we describe the IRI-induced accumulation of structural lipids and the suppression of several metabolic pathways. We report the upregulation of the PPP, which may provide oxidative protection and supply building blocks for cellular regeneration.

MS analysis was used to measure renal lipid accumulation in our murine, unilateral IRI model. Cholesterol, phospholipids, and sphingolipids, all essential constituents of the plasma membrane [30–33], were found to be increased in the kidneys of ischaemic mice. As cellular regeneration and proliferation are required to cope with the IRI-induced necrotic cell death, the demand for plasma membrane production increases.

Unesterified cholesterol acts as a critical regulator of membrane fluidity [30]. CE and FC levels were significantly increased in renal homogenates. Cholesterol exchange/transfer occurs between the plasma membrane and lipoproteins for the removal of CE, which are stored in LDs and the endolysosomal compartment [27,34]. The accumulation of FC may indicate the establishment of a cholesterol reservoir for the building of new membranes.

The effect of renal ischaemia on membrane metabolism has been known for at least three decades. Siegel *et al* quantified the incorporation of [^{14}C]choline into phospholipids as a measurement of membrane metabolism in a rat model of ischaemia and reported a

significant increase in the [^{14}C]choline uptake in ischaemic rats [35]. Among the phospholipids detected by MS analysis, significant accumulation was only observed for PG; however, we also report a trend towards increased PC, PI, and BMP levels. This increment in renal phospholipid levels after ischaemic injury can be associated with enhanced biogenesis of endosomal, lysosomal, mitochondrial, and plasma membranes [36–39].

Sphingolipids are strategically distributed to specific plasma membrane microdomains, serving as platforms for receptor proteins and lipids, and thereby facilitating transmembrane signalling [32,33]. The increased sphingolipid levels observed in ischaemic kidneys may alter plasma membrane microdomain distribution and formation, which consequently impact signalling pathways and lipid-derived second messengers. Particularly ceramide, a central lipid species of the sphingolipid pathway, is involved in multiple intracellular processes, such as cell proliferation, differentiation, cell cycle arrest, and apoptosis [40]. Therefore, besides its role in the renewal of membranes, sphingolipid accumulation is also regarded as a response to cellular stress.

The GSE52004 database allowed us to study the effect of IRI on metabolic pathways within the nephron. We validated these data in renal tissue collected from a bilateral IRI model, as the microarray data were also generated from a bilateral IRI model. We confirmed both proximal and distal tubular injury by quantifying the expression of *Kim-1* and *Ngal*, respectively. The significantly decreased expression of the FAO markers *Ppar-alpha* and *Pcg1-alpha* corresponded to the suppression of the FAO pathway observed in the microarray data. Upregulation of the PPP was validated by measuring the expression of *G6pdx*, *Taldo1*, *Tkt*, and *Prps1*, which encode four enzymes. G6PDX catalyses the rate-limiting step of the oxidative phase of the PPP, while TALDO1, TKT, and PRPS1 are involved in the non-oxidative phase. The upregulation of the PPP was confirmed in our samples, as the expression of all four PPP-related genes was significantly increased in ischaemic mice.

In order to fulfil the continuous demands of active transport, proximal tubular cells exhibit a high rate of metabolic activity. These cells are most reliant on aerobic respiration through OXPHOS and mitochondrial FAO. As both OXPHOS and FAO are suppressed, and the glycolytic capacity of proximal tubules is limited, the proximal tubules effectively lose their energy supply under ischaemic conditions [41] and consequently their function, as reflected by the elevation of urea/creatinine levels following IRI [42].

Twenty-four hours following IRI, LDs, observed as intratubular, perilipin-2-positive vacuoles, were detectable in ischaemic renal tissue [43]. FAs are stored as TAGs through an esterification reaction with glycerol [44], and LDs are known to contain neutral lipids, such as cholesterol esters and TAGs [27]. Therefore, the suppression of FAO, and the resulting FA accumulation, along with the augmented CE levels, may underlie the increase in LD formation in ischaemic kidneys. In light of the reduced mRNA levels of *Fasn* and the FA membrane transporter *Cd36*, FA accumulation following IRI is likely the result of suppressed catabolism rather than active synthesis and/or uptake. Indeed, FA accumulation has been linked to the ischaemia-induced absence of oxidative substrates [45]. Both mitochondrial and peroxisomal FAQ [46] are dependent on oxygen availability. Furthermore, as FAs are a structural component of phospholipids [31], we cannot exclude the remodelling of phospholipids as another possible source of FAs.

Contrary to others, we did not find evidence that indicated an increase in anaerobic glycolysis in ischaemic tubules. A study by Lan *et al* reported a metabolic shift towards anaerobic glycolysis in kidneys that had suffered ischaemic injury. Interestingly, the increase in glycolytic activity was higher in proximal tubules that failed to recover but instead displayed persistent mitochondrial damage and became atrophic [47]. Legouis *et al* have recently shown that AKI leads to increased glycolysis and reduced gluconeogenesis in the kidney, which together lead to lactate accumulation and a decrease in systemic glucose levels. AKI-associated mortality was reduced when glucose metabolism was restored by thiamine supplementation, thereby demonstrating the need to explore metabolic disturbances in AKI as new areas for therapeutic intervention [48].

The PPP, which is related to the glycolytic pathway, consists of an oxidative phase that metabolises glucose to produce NADPH and a non-oxidative phase that produces five-carbon sugars called pentoses. NADPH is a reducing agent that protects against ROS production, which is one of the most prominent sources of renal injury following reperfusion. Pentoses are necessary for nucleotide synthesis during cell proliferation and regeneration. The PPP does not provide any cellular energy but can be redirected towards glycolysis for ATP production. Our data imply that during the reperfusion phase, the cell strategically chooses the PPP over glycolysis. Once metabolic functions have been restored, it does not seem advantageous for the cell to shuttle glucose through a pathway that does not yield ATP; however, our analysis of a single cell RNA dataset [29] showed that increased expression of several PPP-related genes is maintained for up to 7 days following IRI in the proximal tubular cell population. This further suggests that the activation of the PPP may be responsible for the generation of 'chemical supplies' needed for cellular repair.

The anti-oxidative effects of the PPP have been shown to protect neurons during brain IRI [49]. Kim *et al* reported increased PPP activity after renal IRI, as well as its protective effect [50], while Ash and Cuppage described PPP activity in renal homogenates following mercuric chloride injection in rats [51]. Furthermore, a study by Zhou and co-workers reported

that the renoprotective effect of inhibiting the glycolytic pathway following renal ischaemia was mediated by the upregulation of the PPP [52]. Taken together, these studies support the role of the PPP in the regeneration of renal tissue; however, specific inhibition of the PPP in renal IRI is needed to definitively determine the effect of this metabolic pathway and explore its therapeutic potential.

As previously mentioned, renal lipid accumulation has been observed in both acute and chronic renal disease. In terms of chronic renal disease, there seems to be a consensus on the damaging effects of FA [53] and phospholipid [9] accumulation. Although Zager's group has linked ACR in AKI to increased cholesterol content [12], we have shown that renal lipid accumulation following renal IRI is not limited to cholesterol accumulation. Therefore, the overall effect of renal lipid accumulation in AKI remains unclear. Based on this evidence, we can speculate that the net effect of renal lipid accumulation following AKI is based on the cumulative effects of the various lipid types that accumulate. Possibly, temporary intervention in the accumulation of the lipids deemed more detrimental may enhance the effect of the lipids shown to be beneficial. It is, however, crucial to remember that lipid metabolism is linked; therefore targeting one lipid species will often affect another [54]. Interestingly, the upregulation of the PPP in renal ischaemia may be linked to the IRI-induced renal lipid accumulation, as the reducing agent NADPH, a major product of PPP, is necessary for the biochemical pathways involved in both FA and cholesterol synthesis [55,56]. Further investigations are needed to address whether the induction of the PPP and renal lipid storage are causally related.

Our data do not exclude the possibility that other cell types may contribute to renal lipid accumulation following renal IRI; however, we have shown that there is significant lipid accumulation in tubular cells and that this can be linked to the downregulation of several catabolic pathways. We anticipate that the redirection of glucose through the PPP, following IRI, will be beneficial, as this pathway protects against oxidative stress and provides precursors for the biosynthesis of nucleotides and amino acids, both of which are crucial for cell regeneration and the induction of the reparative phase.

Acknowledgements

AS was supported by ZonMW MKMD (grant No 40-42600-98-219). JCL was supported by The Netherlands Organization for Scientific Research (Vidi grant No 91712386). AT is supported by the NOW–FAPESP joint grant on healthy ageing, executed by ZonMw (No 457002002). We would like to thank Professor Andrew P McMahon and Professor Steve S Potter for making their gene expression data publicly available. Mark Dessing is acknowledged for providing the renal samples used for the validation experiments.

Author contributions statement

JR, AT, JCL and SF supervised this project. Study design was the collaborative effort of JR, AT, AS, JCL and SF. Data were collected by ER, LK and GT. Data analysis and interpretation were done by AS, AT, ER, JD and JR. The manuscript was written by AS and reviewed and edited by AS, AT, JCL, ER and JR.

Data availability statement

The microarray and RNAseq datasets displayed in this article were derived from GSE52004 and the scRNA Mouse IRI tool, which can be accessed at https://research.cchmc.org/PotterLab/scIRI/.

References

1. Zarbock A, Gomez H, Kellum JA. Sepsis-induced acute kidney injury revisited: pathophysiology, prevention and future therapies. *Curr Opin Crit Care* 2014; **20:** 588–595.
2. Gameiro J, Fonseca JA, Neves M, *et al*. Acute kidney injury in major abdominal surgery: incidence, risk factors, pathogenesis and outcomes. *Ann Intensive Care* 2018; **8:** 22.
3. Yu L, Seguro AC, Rocha AS. Acute renal failure following hemorrhagic shock: protective and aggravating factors. *Ren Fail* 1992; **14:** 49–55.
4. Ditonno P, Impedovo SV, Palazzo S, *et al*. Effects of ischemia–reperfusion injury in kidney transplantation: risk factors and early and long-term outcomes in a single center. *Transplant Proc* 2013; **45:** 2641–2644.
5. Siedlecki A, Irish W, Brennan DC. Delayed graft function in the kidney transplant. *Am J Transplant* 2011; **11:** 2279–2296.
6. Zager RA, Andoh T, Bennett WM. Renal cholesterol accumulation a durable response after acute and subacute renal insults. *Am J Pathol* 2001; **159:** 743–752.
7. Zager RA, Johnson ACM, Hanson SY. Renal tubular triglycercide accumulation following endotoxic, toxic, and ischemic injury. *Kidney Int* 2005; **67:** 111–121.
8. Braun F, Rinschen MM, Bartels V, *et al*. Altered lipid metabolism in the aging kidney identified by three layered omic analysis. *Aging (Albany NY)* 2016; **8:** 441–457.
9. Rampanelli E, Ochodnicky P, Vissers JP, *et al*. Excessive dietary lipid intake provokes an acquired form of lysosomal lipid storage disease in the kidney. *J Pathol* 2018; **246:** 470–484.
10. Zager RA, Burkhart KM, Johnson ACM, *et al*. Increased proximal tubular cholesterol content: implications for cell injury and 'acquired cytoresistance. *Kidney Int* 1999; **56:** 1788–1797.
11. Zager RA, Kalhorn TF. Changes in free and esterified cholesterol hallmarks of acute renal tubular injury and acquired cytoresistance. *Am J Pathol* 2000; **157:** 1007–1016.
12. Zager RA. 'Biologic memory' in response to acute kidney injury: cytoresistance, toll-like receptor hyper-responsiveness and the onset of progressive renal disease. *Nephrol Dial Transplant* 2013; **28:** 1985–1993.
13. Tammaro A, Kers J, Scantlebery A, *et al*. Metabolic flexibility and innate immunity in renal ischemia reperfusion injury: the fine balance between adaptive repair and tissue degeneration. *Front Immunol* 2020; **11** 1346.
14. Scantlebery AML, Ochodnicky P, Kors L, *et al*. β-Cyclodextrin counteracts obesity in Western diet-fed mice but elicits a nephrotoxic effect. *Sci Rep* 2019; **9:** 17633.

15. Bligh EG, Dyer WJ. A rapid method of total lipid extraction and purification. *Can J Biochem Physiol* 1959; **37:** 911–917.
16. Liebisch G, Lieser B, Rathenberg J, *et al*. High-throughput quantification of phosphatidylcholine and sphingomyelin by electrospray ionization tandem mass spectrometry coupled with isotope correction algorithm. *Biochim Biophys Acta* 2004; **1686:** 108–117.
17. Baker DL, Desiderio DM, Miller DD, *et al*. Direct quantitative analysis of lysophosphatidic acid molecular species by stable isotope dilution electrospray ionization liquid chromatography–mass spectrometry. *Anal Biochem* 2001; **292:** 287–295.
18. Scherer M, Schmitz G, Liebisch G. High-throughput analysis of sphingosine 1-phosphate, sphinganine 1-phosphate, and lysophosphatidic acid in plasma samples by liquid chromatography–tandem mass spectrometry. *Clin Chem* 2009; **55:** 1218–1222.
19. Scherer M, Schmitz G, Liebisch G. Simultaneous quantification of cardiolipin, bis(monoacylglycero)phosphate and their precursors by hydrophilic interaction LC–MS/MS including correction of isotopic overlap. *Anal Chem* 2010; **82:** 8794–8799.
20. Liebisch G, Binder M, Schifferer R, *et al*. High throughput quantification of cholesterol and cholesteryl ester by electrospray ionization tandem mass spectrometry (ESI–MS/MS). *Biochim Biophys Acta* 2006; **1761:** 121–128.
21. Rampanelli E, Orsó E, Ochodnicky P, *et al*. Metabolic injury-induced NLRP3 inflammasome activation dampens phospholipid degradation. *Sci Rep* 2017; **7:** 2861.
22. Liu J, Krautzberger AM, Sui SH, *et al*. Cell-specific translational profiling in acute kidney injury. *J Clin Invest* 2014; **124:** 1242–1254.
23. Ritchie ME, Phipson B, Wu D, *et al*. Limma powers differential expression analyses for RNA-sequencing and microarray studies. *Nucleic Acids Res* 2015; **43:** e47.
24. Yu G He QY. ReactomePA: an R/Bioconductor package for reactome pathway analysis and visualization. *Mol Biosyst* 2016; **12:** 477–479.
25. Jassal B, Matthews L, Viteri G, *et al*. The reactome pathway knowledgebase. *Nucleic Acids Res* 2020; **48:** D498–D503.
26. Zhou G, Soufan O, Ewald J, *et al*. NetworkAnalyst 3.0: a visual analytics platform for comprehensive gene expression profiling and meta-analysis. *Nucleic Acids Res* 2019; **47:** W234–W241.
27. Onal G, Kutlu O, Gozuacik D, *et al*. Lipid droplets in health and disease. *Lipids Health Dis* 2017; **16:** 128.
28. Huang H, van Dullemen LFA, Akhtar MZ, *et al*. Proteometabolomics reveals compensation between ischemic and non-injured contralateral kidneys after reperfusion. *Sci Rep* 2018; **8:** 8539.
29. Rudman-Melnick V, Adam M, Potter A, *et al*. Single-cell profiling of AKI in a murine model reveals novel transcriptional signatures, profibrotic phenotype, and epithelial-to-stromal crosstalk. *J Am Soc Nephrol* 2020; **31:** 2793–2814.
30. Cooper RA. Influence of increased membrane cholesterol on membrane fluidity and cell function in human red blood cells. *J Supramol Struct* 1978; **8:** 413–430.
31. Lombard J. Once upon a time the cell membranes: 175 years of cell boundary research. *Biol Direct* 2014; **9:** 32.
32. Kraft ML. Sphingolipid organization in the plasma membrane and the mechanisms that influence it. *Front Cell Dev Biol* 2017; **4:** 154.
33. Heung LJ, Luberto C, Del Poeta M. Role of sphingolipids in microbial pathogenesis. *Infect Immun* 2006; **74:** 28–39.
34. Aqul A, Liu B, Ramirez CM, *et al*. Unesterified cholesterol accumulation in late endosomes/lysosomes causes neurodegeneration and is prevented by driving cholesterol export from this compartment. *J Neurosci* 2011; **31:** 9404–9413.
35. Siegel MB, Lowenstein LM, Levinsky NG. Choline uptake into renal phospholipids following renal ischemia in rats. *Circ Res* 1979; **44:** 62–67.
36. Colbeau A, Nachbaur J, Vignais PM. Enzymic characterization and lipid composition of rat liver subcellular membranes. *Biochim Biophys Acta* 1971; **249:** 462–492.
37. Osman C, Voelker DR, Langer T. Making heads or tails of phospholipids in mitochondria. *J Cell Biol* 2011; **192:** 7–16.
38. Falkenburger BH, Jensen JB, Dickson EJ, *et al*. Phosphoinositides: lipid regulators of membrane proteins. *J Physiol* 2010; **588:** 3179–3185.
39. Akgoc Z, Iosim S, Seyfried TN. Bis(monoacylglycero)phosphate as a macrophage enriched phospholipid. *Lipids* 2015; **50:** 907–912.
40. Mathias S, Peña LA, Kolesnick RN. Signal transduction of stress via ceramide. *Biochem J* 1998; **335:** 465–480.
41. Balaban RS, Mandel LJ. Metabolic substrate utilization by rabbit proximal tubule. An NADH fluorescence study. *Am J Physiol* 1988; **254:** F407–F416.
42. Basile DP, Anderson MD, Sutton TA. Pathophysiology of acute kidney injury. *Compr Physiol* 2012; **2:** 1303–1353.
43. Yang X, Dunning KR, Wu LL, *et al*. Identification of Perilipin-2 as a lipid droplet protein regulated in oocytes during maturation. *Reprod Fertil Dev* 2010; **22:** 1262–1271.
44. Berg J, Tymoczko J, Stryer L. Fatty acid metabolism. In *Biochemistry* (5th edn), W.H. Freeman and Company: New York, 2002.
45. Portilla D. Role of fatty acid beta-oxidation and calcium-independent phospholipase A2 in ischemic acute renal failure. *Curr Opin Nephrol Hypertens* 1999; **8:** 473–477.
46. Gulati S, Ainol L, Orak J, *et al*. Alterations of peroxisomal function in ischemia–reperfusion injury of rat kidney. *Biochim Biophys Acta* 1993; **1182:** 291–298.
47. Lan R, Geng H, Singha PK, *et al*. Mitochondrial pathology and glycolytic shift during proximal tubule atrophy after ischemic AKI. *J Am Soc Nephrol* 2016; **27:** 3356–3367.
48. Legouis D, Ricksten SE, Faivre A, *et al*. Altered proximal tubular cell glucose metabolism during acute kidney injury is associated with mortality. *Nat Metab* 2020; **2:** 732–743.
49. Cao L, Zhang D, Chen J, *et al*. G6PD plays a neuroprotective role in brain ischemia through promoting pentose phosphate pathway. *Free Radic Biol Med* 2017; **112:** 433–444.
50. Kim J, Devalaraja-Narashimha K, Padanilam BJ. TIGAR regulates glycolysis in ischemic kidney proximal tubules. *Am J Physiol Renal Physiol* 2015; **308:** F298–F308.
51. Ash SR, Cuppage FE. Shift toward anaerobic glycolysis in the regenerating rat kidney. *Am J Pathol* 1970; **60:** 385–402.
52. Zhou HL, Zhang R, Anand P, *et al*. Metabolic reprogramming by the S-nitroso-CoA reductase system protects against kidney injury. *Nature* 2019; **565:** 96–100.
53. Bobulescu IA. Renal lipid metabolism and lipotoxicity. *Curr Opin Nephrol Hypertens* 2010; **19:** 393–402.
54. Ridgway N. Integration of phospholipid and sterol metabolism in mammalian cells. *Prog Lipid Res* 1999; **38:** 337–360.
55. Salati LM, Goodridge AG. Chapter 4 Fatty acid synthesis in eukaryotes. In *New Comprehensive Biochemistry*, *Volume 31*, no. C, Elsevier, 1996; 101–127.
56. Buhaescu I, Izzedine H. Mevalonate pathway: a review of clinical and therapeutical implications. *Clin Biochem* 2007; **40:** 575–584.

SUPPLEMENTARY MATERIAL ONLINE

Supplementary figure legends

Figure S1. IRI-induced renal damage and lipid accumulation in unilateral and bilateral IRI models

Figure S2. Network map of pathways in the nephron affected by IRI

Figure S3. Effect of IRI on the expression of genes involved in metabolic pathways in the nephron (4 – part 1)

Figure S4. Effect of IRI on the expression of genes involved in metabolic pathways in the nephron (4 – part 2)

Figure S5. Effect of IRI on the expression of genes involved in metabolic pathways in the nephron (5)

Figure S6. Glycolysis and the pentose phosphate pathway

Figure S7. Gene expression analysis to investigate the expression of genes related to damage, FAO, and the PPP in the reparative phase following IRI

Table S1. Sequences of the primers used for qPCR